Journal of Power Sources 196 (2011) 4236–4241

Contents lists available at ScienceDirect

Journal of Power Sources

journal homepage: www.elsevier.com/locate/jpowsour

Influence of the synthesis method on the properties of Pt catalysts supported on carbon nanocoils for ethanol oxidation

M.J. Lázaro[a,*], V. Celorrio[a], L. Calvillo[a], E. Pastor[b], R. Moliner[a]

[a] Instituto de Carboquímica (CSIC), Miguel Luesma Castán 4, 50018 Zaragoza, Spain
[b] Departamento de Química Física, Universidad de La Laguna, Avda. Astrofísico Francisco Sánchez s/n, 38071 La Laguna, Tenerife, Spain

ARTICLE INFO

Article history:
Received 7 October 2010
Accepted 11 October 2010
Available online 23 October 2010

Keywords:
Pt electrocatalysts
Carbon nanocoils
Ethanol electrooxidation
DAFC

ABSTRACT

Pt electrocatalysts supported on carbon nanocoils (CNCs) were prepared by the sodium borohydride (BM), formic acid (FAM) and ethylene glycol (EGM) reduction methods in order to determine the influence of the synthesis method on the physicochemical and electrochemical properties of Pt/CNC catalysts. For this purpose, physicochemical properties of these materials were studied by means of energy dispersive X-ray analyses, X-ray diffraction and N_2-physisorption, whereas their electrochemical activity towards ethanol and carbon monoxide oxidation was studied using cyclic voltammetry and chronoamperometry. Furthermore, in order to complete this study, the results obtained for Pt/CNC catalysts were compared with those obtained for Pt catalysts supported on Vulcan XC-72R (commercial support) prepared by the same methods and for the commercial Pt/C catalysts from E-TEK. Results showed that, for all studied methods, CO oxidation occurred at more negative potentials on Pt/CNC catalysts than on Pt/Vulcan and Pt/C E-TEK ones. On the other hand, higher current densities for the ethanol electrooxidation were obtained when CNCs were used as support for BM and EGM. It is concluded that optimizing the synthesis method on CNC, materials with enhanced electrooxidation properties could be developed.

1. Introduction

Low-temperature fuel cells, operated by hydrogen (polymer electrolyte fuel cell, PEMFC), methanol (direct methanol fuel cell, DMFC) or ethanol (direct ethanol fuel cell, DEFC) as fuels, represent an environmentally friendly technology and are attracting much interest as a means of producing electricity by direct electrochemical conversion [1–5]. Direct alcohol fuel cells (DMFCs and DEFCs) have the advantage of running with pure different alcohols mixed with water steam and supplied directly to the anode, eliminating the problems of hydrogen transport and supply. Due to their characteristics, they are promising candidates for portable power source, electric vehicle and transport applications.

The direct oxidation of methanol in fuel cells has been widely investigated. However, the high toxicity of methanol is still an important drawback for their use. In this context, the use of ethanol as fuel seems to be a possible solution to this problem, due to it is not toxic and can be produced in large quantities from agricultural products (bioethanol) [1,6,7]. Furthermore, ethanol provides a volumetric energy density (21 MJ l^{-1}) that approaches that of gasoline (31 MJ l^{-1}).

In the case of methanol, many efforts have been done during the past decades to establish not only the oxidation reaction mechanism, but also the type of electrocatalyst to be used as anode material. However, in the case of ethanol, nowadays, it is difficult to establish the appropriate catalyst to oxidize it electrochemically. Besides platinum, other metals have been studied for the electrooxidation of ethanol, such as gold, rhodium or palladium, and they have shown some activity. However, only platinum-based materials show appropriate oxidation currents, especially in acid medium [8], but the efficiency of the DAFCs operating with these catalysts is still insufficient for practical applications. Therefore, further optimization of the anode material for DAFCs is necessary for their development and commercialisation.

The utilization of nanostructured carbonaceous materials as catalyst supports has been proposed as a promising solution to improve the efficiency and durability of electrocatalysts, due to carbon supports have been found to strongly influence the properties of metal supported nanoparticles, such as metal particle size, morphology, size distribution, stability and dispersion [9]. The ideal support material for fuel cell electrocatalysts should have at least the following characteristics: (i) high electrical conductivity to facilitate electron transport during the electrochemical reactions; (ii) high specific surface area in order to achieve large metal dispersions (which usually results in a high catalytic activity); (iii) suitable mesoporous structure for a good diffusion of reactant and by-products to and from the catalyst; and (iv) presence of surface oxygen groups for a good interaction between the catalysts nanoparticles and the carbon support [10].

* Corresponding author. Tel.: +34 976 733977; fax: +34 976 733318.
E-mail address: mlazaro@icb.csic.es (M.J. Lázaro).

0378-7753/$ – see front matter © 2010 Elsevier B.V. All rights reserved.
doi:10.1016/j.jpowsour.2010.10.055

Vulcan XC-72(R) is the most commonly used electrocatalyst support due to its high electrical conductivity and appropriate textural properties [11,12]. However, it has a considerable content of micropores (~30% of total area) which difficult the access of the fuel. For this reason, a portion of metal nanoparticles could be sunk into the micropores and may have less or no electrochemical activity due to the difficulty in reactant accessibility. Thus, nowadays, novel non-conventional carbon supports with mesoporous structure, such as carbon nanotubes and nanofibers [13,14], carbon xerogels and aerogels [15,16], ordered mesoporous carbons [5] and carbon nanocoils [17] are being studied.

Carbon nanocoils (CNCs) have recently received great attention as catalytic support in fuel cell electrodes due to the combination of their good electrical conductivity, derived from their graphitic structure, and a wide porosity that allows the diffusional resistances of reactants/products to be minimized. Only few works have been performed on catalysts supported on carbon nanocoils for their use both at the anode and cathode side of a direct methanol fuel cell [17–23]. Hyeon et al. synthesized Pt/Ru (1:1) alloy catalyst (60% wt.), prepared by sodium borohydride reduction method, supported on CNCs. They studied its behaviour towards the methanol oxidation, showing its good electrocatalytic activity [17]. Sevilla et al. also demonstrated the high catalytic activity of PtRu/CNC electrocatalyst for the methanol oxidation [18]. In addition, they compared its activity to that of a Pt/Vulcan catalyst prepared by the same method, demonstrating that catalysts supported on CNCs exhibited a higher utilization of metals [19,20]. Park et al. employed carbon nanocoils with variable surface areas and crystallinity as Pt/Ru catalyst supports [21,22]. They found that catalysts supported on carbon nanocoils exhibited better electrocatalytic performance towards the methanol electrooxidation than the catalyst supported on Vulcan XC-72. On the other hand, Imran Jafri et al. studied the activity of Pt nanoparticles dispersed on multi-walled carbon nanocoils for the oxygen reduction reaction in proton-exchange membrane fuel cells [23], the results obtained support the use of this new type of catalyst support material for PEMFC.

The most extended methods for preparing carbon-supported catalysts are the impregnation, the colloidal and the microemulsion methods [4,24]. The most widely used is the impregnation method due to its simplicity and good results. It consists of an impregnation step followed by a chemical reduction step (in liquid or gas phase). It has been found that the catalyst synthesis method can affect the composition, morphology and dispersion of the catalysts, as well as their electrocatalytic performance [25]. However, scarce works about the comparison of catalysts synthesized by different methods can be found in the literature [26], none about carbon nanocoils.

In this paper, Pt catalysts supported on carbon nanocoils produced by the catalytic graphitization of resorcinol-formaldehyde gel [27] have been synthesized. The metal nanoparticles were deposited on the carbon support following formic acid [26,27], sodium borohydride [5] or etilenglicol [28] reduction methods. The aim of this study is to compare different synthesis procedures in order to determine their influence on the properties of catalysts and to obtain an effective catalyst. These results were also compared to the same catalysts supported on Vulcan XC-72, demonstrating that the use of this non-conventional carbon material (CNCs) can improve the performance of the DEFC.

2. Experimental methods

2.1. Synthesis of carbon supports

Carbon nanocoils were synthesized by the catalytic graphitization of resorcinol-formaldehyde gel as described in [27]. In a typical synthesis, formaldehyde (Sigma–Aldrich) and silica sol (Supelco) were disolved in 100 mL of deionized water, then a mixture of nickel (Panreac) and cobalt (Sigma–Aldrich) salts was added under stirring conditions. Subsequently, resorcinol (Sigma–Aldrich) was added, and the stirring conditions maintained for 0.5 h. After a heat treatment at 85 °C for 3 h in a closed system of this reaction mixture, the system was then opened, and the mixture dried at 108 °C. Finally it was carbonized in a nitrogen atmosphere at 900 °C for 3 h. A 5 M NaOH (Panreac) solution was used to remove silica particles, followed by a treatment with concentrated HNO_3 (65%, Fluka) at room temperature during 2 h to remove the metal salts.

2.2. Preparation of the carbon-supported Pt electrocatalysts

The carbon supported Pt electrocatalysts were prepared by formic acid (FAM), sodium borohydride (BM) and ethylene glycol (EGM) reduction methods. Appropiate concentrations of the metal precursor were used to obtain a theoretical platinum loading of 20 wt.% on the different carbon materials. Chloroplatinic acid (8 wt.% $H_2PtCl_6{\cdot}6H_2O$ solution, Sigma–Aldrich) was used as metal precursor.

FAM method involved the suspension of the carbon material in a 2 M formic acid solution (98%, Panreac) and the slowly addition of the chloroplatinic acid solution under stirring conditions at 80 °C [26,27].

In the BM reduction method, catalysts were prepared by impregnating the carbon supports with an 8 wt.% chloroplatinic acid solution. Subsequently, the metal was reduced with a 26.4 mM sodium borohydride solution (99%, Sigma–Aldrich), which was slowly added to the precursor solution under sonication [5].

In the EGM reduction method, ethylene glycol was used as solvent and reducing agent. In a typical procedure, the metal precursor was dissolved in ethylene glycol (1 mL EG/1 mg Pt) and the pH was adjusted to 11 using a 1 M NaOH solution in EG. Then, the carbon support was added. The resulting mixture was treated at 195 °C for 2 h and then cooled in a cold water bath. The pH was measured and adjusted to 1 using HCl (37%, Sigma–Aldrich) [28].

The catalysts were named Pt/CNC or Pt/Vulcan if they are supported on carbon nanocoils or Vulcan XC-72R respectively, followed by the abbreviation of the method used for synthesized them (-FAM, -BM, or -EGM).

2.3. Physicochemical characterization of Pt/C electrocatalysts

The real content of Pt in the electrocatalysts was determined by energy dispersive X-ray analyses (EDX) technique Röntec XFlash Si(Li), coupled to a scanning electron microscopy Hitachi S-3400 N.

X-ray diffraction (XRD) patterns were recorded using a Bruker AXS D8 Advance diffractometer with a θ–θ configuration and using Cu Kα radiation (λ = 0.154 nm). Scans were done for 2θ values between 0° and 100°. Scherrer's equation was applied to the (2 2 0) peak of the Pt fcc structure, around 2θ = 70°, in order to estimate the Pt crystallite size from the diffractograms [29]. This region was chosen to avoid the influence of a broad band of the carbon substrate (2θ = 25°) on the (1 1 1) and (2 0 0) peaks of Pt structure [30,31].

2.4. Electrochemical characterization of Pt/C electrocatalysts

Electrochemical experiments were carried out in a three-electrode cell using a MicroAutolab potentiostat. The counter electrode was a large area pyrolitic graphite bar and a reversible hydrogen electrode (RHE) placed inside a Luggin capillary was used as reference one. All potentials in this work are referred to this electrode. Working electrodes were prepared depositing a thin-layer of the electrocatalysts over a pyrolitic graphite disk (7 mm diameter, 1.54 cm^2 geometric area). A catalyst ink was prepared by

mixing 2 mg of the catalyst and 10 μl of Nafion dispersion (5 wt.%, Aldrich) in 500 μl of ultrapure water (Millipore Milli-Q system). A 40 μl aliqout of the suspension was deposited onto the graphite disk and dried. After that, the working electrode was immersed into H_2SO_4 0.5 M electrolyte solution, prepared from high purity reagents (Merck) and deaerated with nitrogen gas. All the electrochemical experiments presented in this work were carried out at room temperature.

Electrochemical active areas of catalysts were measured from CO-stripping voltammograms by the integration of the CO_{ad} oxidation region, assuming a charge of 420 μC cm^{-2} involved in the oxidation of a monolayer of linearly adsorbed CO. This electroactive area has been used to calculate the current densities given in the text. CO (99.99%, Air Liquide) adsorbs onto the metal surface by bubbling this gas at 1 atm though the electrolyte during 10 min to achieve full monolayer coverage of CO on Pt. The CO adsorption process was carried out at 0.20 V. Then an inert gas such as nitrogen is used to purge out for a few minutes the CO from the solution, leaving only the CO adsorbed on the surface of Pt. A potential scanning between 0.05 and 1.10 V at 0.02 V s^{-1} was then carried out to induce the oxidation of CO for two complete oxidation/reduction scans.

Ethanol oxidation was characterized by cyclic voltammetry and chronoamperometry. Cyclic voltammograms (CVs) were recorded in 2 M CH_3CH_2OH + 0.5 M H_2SO_4 between 0.05 and 1.10 V at a scan rate of 0.02 V s^{-1}. Potentiostatic current density–time (j–t) curves were recorded in the same solutions at 0.60 V for 900 s.

3. Results and discussion

3.1. Physicochemical characterization of the supports and electrocatalysts

Catalysts are usually supported on a carbonaceous material to reduce the amount of metal used and improve its performance. It has been shown that carbonaceous support has great influence on the properties of the catalyst [32]. The physicochemical characterization of the CNC was stated in a previous work [27]. Carbon nanocoils consist of a long curved ribbon of carbon which exhibited well-aligned graphitic layers. Nevertheless, Vulcan XC-72 consisted of an aggregation of spherical carbon nanoparticles.

Table 1 shows the nomenclature and the metal content obtained by EDX for the catalysts prepared and the commercial catalysts Pt/C from E-TEK. The values obtained are similar to the nominal value of 20%.

The textural properties of the supports and the catalysts were studied by N_2-physisorption to determine the effect of the deposition of metal particles on the pore structure of the support (Table 2). CNC had a specific surface area and pore volume of 124 m^2 g^{-1} and 0.16 m^3 g^{-1}, respectively, and a mesoporous structure, whereas Vulcan XC-72R had a specific surface area of around 218 m^2 g^{-1} and a total pore volume of 0.41 m^3 g^{-1}, being the 30% of its area belonging to the micropores. Metal particles deposited in the micropores of this material may have a lower electrocatalytic activity, or even not to operate, because of the worst diffusion of reagents through this structure to the active sites.

Table 1
Pt content from EDX and physical characteristics from XRD analysis of the catalysts.

Electrocatalyst	% Pt	d (nm)	Latticce parameter (Å)	Metal surface area (m^2 g^{-1})
Pt/CNC-BM	20.0	4.7	3.9198	60
Pt/CNC-EGM	16.2	5.6	3.9158	50
Pt/CNC-FAM	19.4	3.8	3.9233	74
Pt/Vulcan-BM	17.3	3.7	3.9029	76
Pt/Vulcan-EGM	20.0	5.4	3.9174	52
Pt/Vulcan-FAM	19.2	3.2	3.9158	88
Pt/C E-TEK	16.3	3.0	3.9231	93

Table 2
Textural parameters of carbon supports and catalysts.

Sample	S_{BET} (m^2 g^{-1})	V_{Total} (cm^3 g^{-1})	$S_{Mesopore}$ (m^2 g^{-1})	$S_{Micropore}$ (m^2 g^{-1})
CNC	124	0.16	124	0.0
Vulcan	218	0.41	153	65

The morphological and crystallographic properties of the catalysts were studied by X-ray diffraction (XRD). X-ray diffractograms for Pt/C electrocatalysts are shown in Fig. 1. All of them showed the typical form of the face-centered cubic (fcc) Pt structure, indicating the effective reduction of the metal precursor producing crystalline nanoparticles. Peaks at $2\theta = 40^\circ$, 47°, 67°, 81° and 85°, associated with the Pt crystal planes (1 1 1), Pt (2 0 0), Pt (2 2 0), Pt (3 1 1) and Pt (2 2 2), respectively, were observed. Furthermore, the XRD patterns displayed a peak at $2\theta = 26.2^\circ$, characteristic of the plane (0 0 2) of graphite, which is attributed to the CNCs used as support. In the case of Pt/Vulcan and commercial catalysts, the peak attributed to the support was less intense due to the lower crystalline grade of Vulcan XC-72R. Both metal crystallite size and specific activity are influenced by the interaction of the active phase with the support as will be seen below.

Average metal crystallite sizes, calculated from the Scherrer' equation, are given in Table 2. Differences in the Pt average crystallite sizes were observed for the different carbon supports and synthesis methods. Higher Pt average sizes were obtained as CNCs were used as support, compared with those obtained using Vulcan XC-72R. However, these differences were not significant. This could be attributed to that Vulcan XC-72R has a large number of nucleation sites, leading to the formation of smaller Pt particles. In contrast, graphitized carbons, like CNCs, have a lower number of nucleation sites because only the surface defects can function as nucleation sites, and thus larger Pt particles would be obtained. However, for both carbon materials, the smallest particle size was obtained by FAM and the highest ones by EGM.

The surface area (SA) can be calculated (Table 2), assuming that Pt particles are spherical, by the ratio SA (m^2 g^{-1}) = $6 \times 10^3/\rho d$, where d is the mean metal crystallite size in nm, and ρ is the density of Pt (21.4 g cm^{-3}). Different values were obtained using CNCs as support modifying the metal precursor reducing agent. Of those methods, the catalysts synthesized by FAM presented a smaller

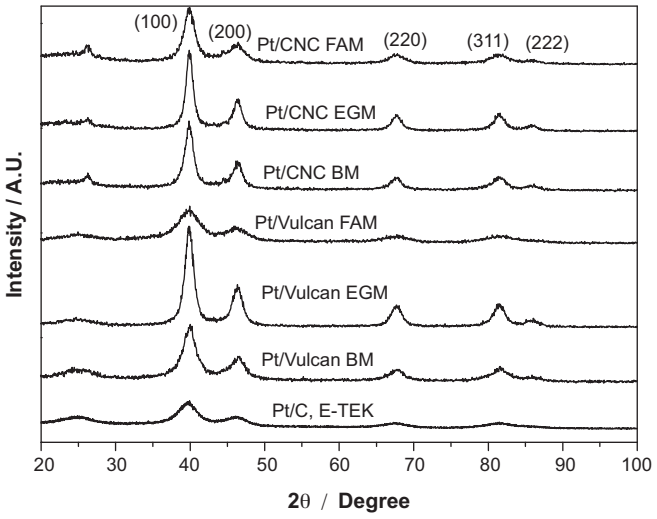

Fig. 1. XRD diffractograms for the Pt electrocatalysts supported on CNCs and Vulcan XC-72R, including the Pt/C E-TEK catalyst.

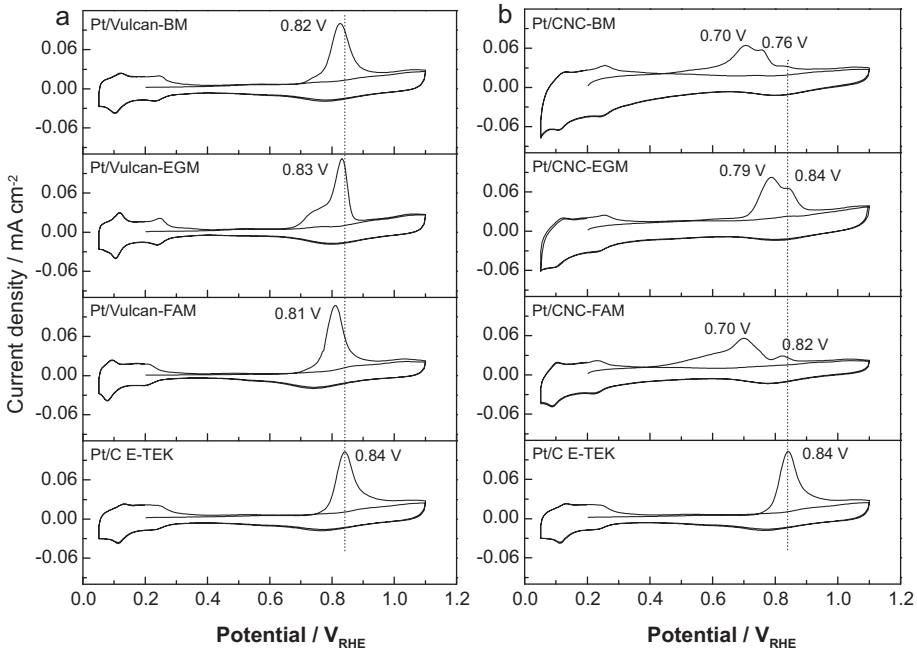

Fig. 2. CO-stripping voltammetries for Pt/Vulcan (a) and Pt/CNC (b) electrocatalysts in 0.5 M H_2SO_4. E_{ad} = 0.20 V; υ = 20 mV s^{-1}; T = 25 °C.

crystal size and, therefore, a greater metal surface area, opposite to EGM.

The lattice parameter was also calculated from XRD patterns and the results are summarized in Table 1. The value of the lattice parameter of the Pt/C electrocatalysts decreases with increasing the crystallite size. These values were close to 3.92 Å, which is the value correspondent to pure platinum.

3.2. Electrochemical studies

3.2.1. Carbon monoxide oxidation

CO-stripping voltammetry can be used to obtain some in situ information about the electroactive composition and surfaces areas of catalysts, as well as, to establish their tolerance towards CO poisoning. CO-stripping voltammograms obtained at room temperature are shown in Fig. 2, where the first and second cycles are represented. As observed, in the first cycle, when the Pt surface is blocked by the CO adsorbed, hydrogen adsorption is blocked. Therefore, the cyclic voltammogram in the hydrogen adsorption–desorption potential region becomes featureless. Once the CO monolayer is removed through oxidation at higher potentials, the Pt surface becomes available again for hydrogen adsorption and desorption, and the corresponding peaks appear (corresponding to the voltammograms in the base electrolyte for the clean surfaces) in the second cycle.

Similar results were obtained for Pt/Vulcan and commercial Pt/C E-TEK catalysts. As can be seen in Fig. 2a, the peak potential for the CO_{ad} oxidation occurred approx. at the same potential for Pt/C E-TEK and Pt/Vulcan catalysts, in the 0.81–0.84 potential range. However, the onset for CO oxidation was placed of CO started at more negative potentials for Pt/Vulcan catalysts (around 0.7 V) than for Pt/C E-TEK one (0.76 V). No significant differences were observed for the Pt/Vulcan catalysts synthesized by different methods, only for the Pt/Vulcan-EGM a shoulder centred at 0,72 V is apparent which implies that for this catalyst part of CO oxidation occurs at more negative potentials.

In the case of Pt/CNC catalysts, the oxidation of CO_{ad} is shifted negatively compared with Pt/Vulcan and Pt/C E-TEK catalysts (Fig. 2b). For these catalysts, two CO oxidation peaks were observed in the CVs. One peak around 0.84 V was observed, which corresponds to that observed for catalysts supported on Vulcan XC-72R. In addition, a second CO oxidation peak was obtained at around 0.70 V for Pt/CNC-BM and Pt/CNC-FAM and at 0.79 V for Pt/CNC-EG. This implies that CO can be easily oxidized on these materials. The presence of this additional peak at lower potentials could be attributed to the nature and surface chemistry of the carbon support, specifically to the surface oxygen groups of the CNCs [1,33], which could alter the electronic structure of the metal, helping to the CO oxidation process and making catalysts more tolerant to CO than Vulcan-supported catalysts.

It is noticeable the presence of an important CO oxidation current at E < 0.60 V for catalysts prepared on CNC by BM and FAM, especially for the latter, which implies that CO can be oxidized at potentials as low as 0.40 V at Pt on CNC.

However, as can be observed in Fig. 2b, the ratio between the two peak areas varied with the synthesis method. This demonstrates that the deposition method of the metal particles plays an important role in the final performance of the electrocatalysts.

3.2.2. Ethanol oxidation

Fig. 3 illustrates the CVs recorded in 2 M CH_3CH_2OH + 0.5 M H_2SO_4 at room temperature for Pt/CNC, Pt/Vulcan and commercial Pt/C E-TEK catalysts. The curves for all catalysts displayed a rise in the current around 0.50 V during the positive-going potential scan, developing an anodic peak which position depends on the catalysts. At the backward scan, a new anodic contribution was observed, achieving a maximum also dependent on the catalyst.

As can be observed in Fig. 3, the onset for ethanol electrooxidation occurred between 0.50 and 0.64 V depending on the catalysts. For the same material, significant differences were found in the current densities achieved for the catalysts prepared following the different synthesis methods. In the case of Pt/CNC catalysts, the highest current densities were observed for the Pt/CNC-BM (1.1 mA cm^{-2}), whereas in the case of Pt/Vulcan ones, Pt/Vulcan-FAM (0.7 mA cm^{-2}) showed the highest current densities during the positive potential scan. In all cases, higher current densities than those for Pt/C E-TEK (0.2 mA cm^{-2}) were obtained.

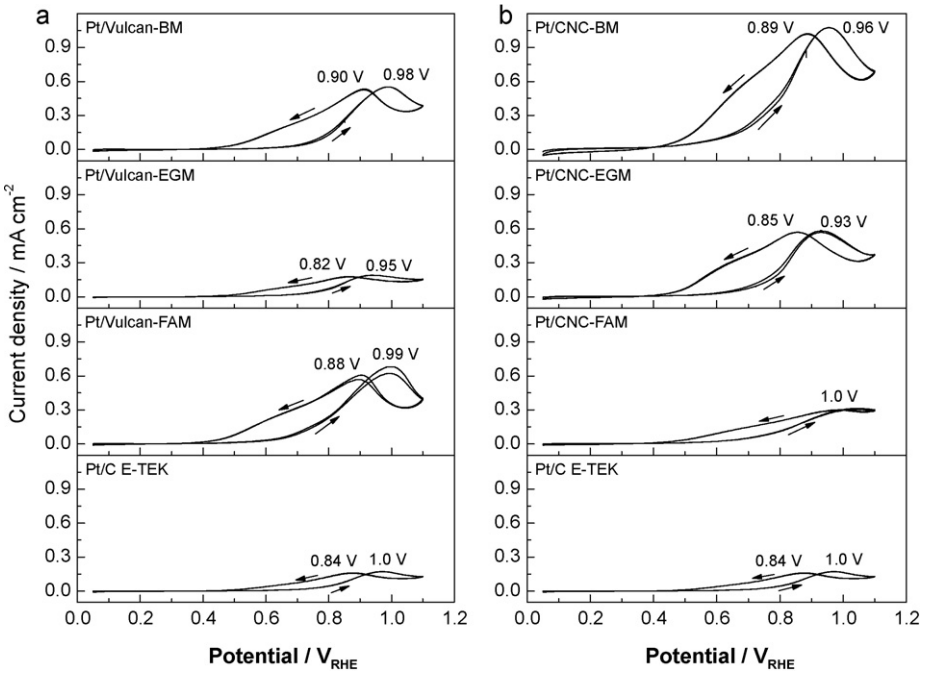

Fig. 3. Cyclic voltammograms for Pt/Vulcan (a) and Pt/CNC (b) electrocatalysts in 2 M CH_3CH_2OH + 0.5 M H_2SO_4. υ = 20 mV s^{-1}; T = 25 °C.

Table 3
Current densities obtained from cyclic voltammetry (CV) and chronoamperometric (CR) curves for Pt/C catalysts in 2 M CH_3CH_2OH + 0.5 M H_2SO_4 solution at 0.60 V.

Electrocatalyst	$CV_{0.60}$ ($\mu A\,cm^{-2}$)	$CR_{0.60}$ ($\mu A\,cm^{-2}$)
Pt/CNC-BM	110	47
Pt/CNC-EGM	33	33
Pt/CNC-FAM	22	21
Pt/Vulcan-BM	13	18
Pt/Vulcan-EGM	8	12
Pt/Vulcan-FAM	27	21
Pt/C E-TEK	6	5

The current densities obtained for the different catalysts at 0.60 V (a potential near to the working potential in a DEFC) are listed in Table 3.

From Fig. 3, it is demonstrated that the utilization of CNCs as catalysts support results in an increase of the current densities registered at the maximum in the CVs for BM and EGM. The onset potential for the oxidation of ethanol during the positive-going potential scan on Pt/CNC-BM appears at the most negative potential whereas the most positive corresponds to Pt/CNC-FAM. Accordingly, the maximum current density at the first peak of the ethanol electrooxidation is achieved for Pt/CNC-BM, followed by Pt/CNC-EGM, Pt/CNC-FAM and Pt/C E-TEK. It is clear that Pt/CNC-BM presents a higher positive peak current density, and consequently, higher activity to ethanol electro-oxidation which indicates that it is a promising catalyst for ethanol electrooxidation.

Interestingly, Pt/Vulcan catalysts showed higher oxidation activity than the commercial Pt/C E-TEK. This improvement could be attributed to the catalysts preparation method.

With the purpose to determine the performance of the catalysts towards ethanol electrooxidation under potentiostatic conditions, current–time curves were recorded at 0.60 V and 25 °C during 850 s in a 2 M CH_3CH_2OH + 0.5 M H_2SO_4 solution. Fig. 4 shows such curves for the Pt-supported catalysts. Pt catalysts based on CNCs prepared by BM and EGM presented higher quasi-stationary current densities from chronoamperometric curves than Pt catalysts based on Vulcan XC-72R. These values increased in the order Pt/C E-TEK < Pt/Vulcan-EGM < Pt/Vulcan-BM < Pt/Vulcan-FAM = Pt/CNC-FAM < Pt/CNC-EGM < Pt/CNC-BM as can be seen in Table 3. However, in all cases, a stable performance was achieved in a short time.

These results confirm that the Pt/CNC catalysts are notably more active for electrooxidizing ethanol than catalysts supported on Vulcan XC-72R, commonly employed for DAFCs technical electrodes.

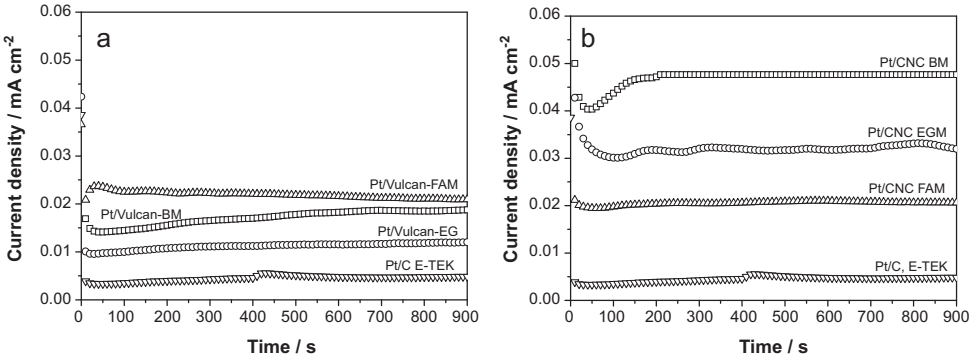

Fig. 4. Chronoamperometric curves for Pt/Vulcan (a) and Pt/CNC (b) electrocatalysts recorded in 2 M CH_3CH_2OH + 0.5 M H_2SO_4 solution at E = 0.60 V.

4. Conclusions

The main conclusions derived from this work can be summarized as follows:

- The size of the platinum crystallites depends on the synthesis method used to prepare the catalysts. For both carbon materials used as support, the FAM resulted in the smallest metal crystallite sizes, whereas the EGM resulted in the highest ones. For each the synthesis methods, higher platinum crystallite size was obtained as CNCs were used as support, respect to that obtained using Vulcan, although differences were no significant. This effect could be attributed to the less content of nucleation sites in CNCs due to their graphitic nature.
- Pt electrocatalysts supported on carbon nanocoils showed more negative CO oxidation potentials compared with catalysts supported on Vulcan and the commercial Pt/C E-TEK one. This can be attributed to the carbon nanocoils used as catalyst support, which could alter the electronic structure of the metal, helping to the CO oxidation process and making catalysts more tolerant to CO than Vulcan-supported ones. On the other hand, differences in the CO oxidation were observed for the catalysts synthesized by different methods, demonstrating that the deposition method of the metal particles plays an important role in the final performance of the electrocatalysts.
- Catalysts based on carbon nanocoils were also notably more active for electrooxidizing ethanol than catalysts supported on Vulcan XC-72R, commonly employed as anodes in DEFCs, which can be also attributed to the positive effect of carbon nanocoils as support. The highest current densities were achieved by the Pt/CNC-BM catalyst.

These results prove that the Pt/CNC catalysts are promising candidates as alternative to replace Pt/Vulcan in order to improve the performance of the direct ethanol fuel cells.

Acknowledgment

The authors gratefully acknowledge financial support given by the MICINN and Gobierno Autónomo de Canarias through Projects MAT2008-06631-C03-01 and MAT2008-06631-C03-02, and PI2007/023, respectively. V. Celorrio and L. Calvillo and also acknowledge CSIC and the Spanish National Research Council for their JAE and FPI grants, respectively.

References

[1] E. Antolini, Appl. Catal. B: Environ. 88 (2009) 1–24.
[2] S. Song, P. Tsiakaras, Appl. Catal. B: Environ. 63 (2006) 187–193.
[3] E. Antolini, J. Power Sources 170 (2007) 1–12.
[4] H. Liu, C. Song, L. Zhang, J. Zhang, H. Wang, D.P. Wilkinson, J. Power Sources 155 (2006) 95–110.
[5] L. Calvillo, M.J. Lázaro, E. García-Bordejé, R. Moliner, P.L. Cabot, I. Esparbé, E. Pastor, J.J. Quintana, J. Power Sources 169 (2007) 59–64.
[6] G. Andreadis, P. Tsiakaras, Chem. Eng. Sci. 61 (2006) 7497–7508.
[7] S.Q. Song, W.J. Zhou, Z.H. Zhou, L.H. Jiang, G.Q. Sun, Q. Xin, V. Leontidis, S. Kontou, P. Tsiakaras, Int. J. Hydrogen Energy 30 (2005) 995–1001.
[8] P.E. Tsiakaras, J. Power Sources 171 (2007) 107–112.
[9] L. Calvillo, M. Gangeri, S. Perathoner, G. Centi, R. Moliner, M.J. Lázaro, J. Power Sources 192 (2009) 144–150.
[10] A.L. Dicks, J. Power Sources 156 (2006) 128–141.
[11] K. Wikander, H. Ekström, A.E.C. Palmqvist, A. Lundblad, K. Holmberg, G. Lindbergh, Fuel Cells 6 (2006) 21–25.
[12] Y. Shao, G. Yin, J. Zhang, Y. Gao, Electrochim. Acta 51 (2006) 5853–5857.
[13] C. Paoletti, A. Cemmi, L. Giorgi, R. Giorgi, L. Pilloni, E. Serra, M. Pasquali, J. Power Sources 183 (2008) 84–91.
[14] H. Tang, J. Chen, L. Nie, D. Liu, W. Deng, Y. Kuang, S. Yao, J. Colloid Interface Sci. 269 (2004) 26–31.
[15] N. Job, J. Marie, S. Lambert, S. Berthon-Fabry, P. Achard, Energy Convers. Manage. 29 (2008) 2461–2470.
[16] J. Marie, S. Berthon-Fabry, P. Achard, M. Chatenet, A. Pradourat, E. Chainet, J. Non-Cryst. Solids 350 (2004) 88–96.
[17] T. Hyeon, S. Han, Y.E. Sung, K.W Park, Y.W. Kim, Angew. Chem. Int. Ed. 42 (2003) 4352–4356.
[18] M. Sevilla, G. Lota, A.B. Fuertes, J. Power Sources 171 (2007) 546–551.
[19] M. Sevilla, C. Sanchís, T. Valdés-Solís, E. Morallón, A.B. Fuertes, Electrochim. Acta 54 (2009) 2234–2238.
[20] M. Sevilla, C. Sanchís, T. Valdés-Solís, E. Morallón, A.B. Fuertes, Carbon 46 (2008) 931–939.
[21] K.W. Park, Y.E. Sung, S. Han, Y. Yun, T. Hyeon, J. Phys. Chem. B 108 (2004) 939–944.
[22] S. Han, Y. Yun, K.-W. Park, Y.-E. Sung, T. Hyeon, Adv. Mater. 15 (2003) 1922–1925.
[23] R. Imran Jafri, N. Rajalakshmi, S. Ramaprabhu, J. Power Sources 195 (2010) 8080–8083.
[24] Z. Liu, X.Y. Ling, X. Su, J.Y. Lee, L.M. Gan, J. Power Sources 149 (2005) 1–7.
[25] J.R.C. Salgado, F. Alcaide, G. Álvarez, L. Calvillo, M.J. Lázaro, E. Pastor, J. Power Sources 195 (2010) 4022–4029.
[26] J.R.C. Salgado, J.J. Quintana, L. Calvillo, M.J. Lázaro, P.L. Cabot, I. Esparbé, E. Pastor, Phys. Chem. Chem. Phys. 10 (2008) 6796–6806.
[27] V. Celorrio, L. Calvillo, M.V. Martínez-Huerta, R. Moliner, M.J. Lázaro, Energy Fuels 24 (2010) 3361–3365.
[28] X. Wang, I.M. Hsing, Electrochim. Acta 47 (2002) 2981–2987.
[29] B.E. Warren, X-ray Diffraction, Addison-Wesley, Reading, 1969.
[30] S. Kim, S.-J. Park, Electrochim. Acta 52 (2007) 3013–3021.
[31] W. Li, W. Zhou, H. Li, Z. Zhou, G. Sun, Q. Xin, Electrochim. Acta 49 (2004) 1045–1055.
[32] T.S. Ahmadi, Z.L. Wang, T.C. Green, A. Henglein, M.A. El-Sayed, Science 272 (1996) 1924–1925.
[33] X. Yu, S. Ye, J. Power Sources 172 (2007) 133.